Proceedings of the 2014 IEEE
International Conference on Robotics and Biomimetics
December 5-10, 2014, Bali, Indonesia

Design of Cluster Geometries for Clusterwheel IP Robots: Obstacle size and Controllability

Hari Vasudevan, *Student Member, IEEE*, Aaron M. Dollar, *Senior Member, IEEE* and John B. Morrell

Abstract— In this paper we discuss issues related to the design of clusterwheel inverted pendulum balancing machines, with a particular focus on the choice of the number of wheels in the cluster. This class of vehicles holds the promise of incorporating the inherent compliance of a two-wheeled balancing vehicle, the stability of a four-wheeled vehicle when desired, and the capability of legs to overcome obstacles such as stairs and indoor terrain. In order to arrive at a design compromise that can retain the advantages of each mode while minimizing disadvantages, we examine the dynamics and control of various cluster geometries and give analytical arguments in support of a three wheel cluster design while verifying our hypothesis using simulations of various cluster architectures. We then present the design and the construction of "Charlie," a prototype clusterwheel vehicle, and demonstrate basic stable obstacle traversal.

I. INTRODUCTION

There are many parts of the human environment that are daunting for robots. Objects of everyday interaction such as stairs, doors, and curbs are often insurmountable obstacles. A wide range of robots have been designed to address specific challenges in human environments, however the versatility and adaptability of human locomotion remains unmatched. While wheeled vehicles have excellent energy efficiency and can be designed to have fairly low mechanical complexity, they fail to provide much adaptability to uneven ground with obstacles greater than approximately quarter of the wheel diameter difficult to surmount. Legged vehicles, on the other hand, are able to pick up their ground contacts in order to overcome obstacles, but require fairly complex mechanical structures and typically many more actuators. Furthermore, traditional vehicles of both kinds (wheeled and legged) tend to be large, rigid, and of high-impedance, making their movements around humans potentially unsafe.

One promising direction that has been actively investigated in the past decade or so is wheeled balancing inverted pendulum platforms [1]–[6], which have the efficiency of wheeled vehicles, but have much greater mobility and smaller footprint. However, they still lack the ability of legged vehicles to overcome significant obstacles. In this paper, we discuss issues related to a class of dynamically balancing inverted pendulum (IP) robots with clusterwheels that allow the platform to switch from balancing (on two wheels) to a more stable four-wheeled configuration. The configuration

H. Vasudevan, and A. M. Dollar are with the Department of Mechanical Engineering and Materials Science, Yale University, New Haven, CT USA `hari.vasudevan,aaron.dollar@yale.edu`.

John B. Morrell was Assistant Professor in the Dept. of Mechanical Engineering and Materials Science, Yale University, New Haven, CT. `john.morrell@alum.mit.edu`
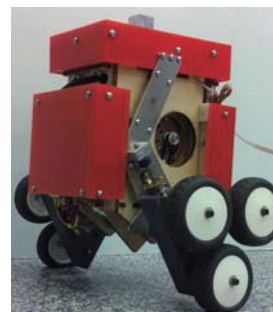
Fig. 1. Charlie balancing on two wheels

allows the robot to negotiate curbs, stairs and walkways commonly encountered in indoor and outdoor built-for-human environments, as well as balance dynamically and remain compliant in order to absorb collisions with humans or other objects in the environment. We particularly examine the effect of changing the number of wheels in the clusters on the stability of the vehicle.

Clusterwheel balancing platforms were previously implemented in the iBOT Mobility System [7]–[13], an advanced powered wheelchair developed in part by co-author Morrell. While the iBOT system demonstrated the feasibility and benefits of the concept, there are still many aspects of the design and control of these types of vehicles left unexplored. These include optimal cluster geometries, actuator specifications and dynamic control of the robot during transitions between 2-wheeled (balancing) and 4-wheeled modes. This paper investigates a key issue in the design of these systems: how the selection of cluster geometry affects the controllability of the vehicle as well as the ability to overcome obstacles such as stairs.

Besides balancing platforms, other work on multi-functional locomotion designed for both movement and terrain climbing can broadly be categorized into three architectures, legged, wheeled and treaded. A detailed taxonomy of robot locomotion is surveyed by Whittaker et al. [14]. A combination of leg-wheel hybrids have also been designed, combining the efficiency of wheels with the terrain capability of legs. The Whegs [15] platform is a prominent example of the legs on wheels concept while the Scarab [14], Octopus [16] are examples of wheels on legs. There also exists a number of treaded robots designed to climb stairs and other obstacles in human environments. S.Hirose et al. [17] describe a tread mechanism with flaps attached to treads and a tail that can successfully climb stairs, additionally there exists other literature [18]–[20] on stair climbing on
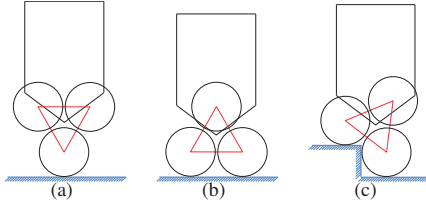
Fig. 2. Various intended modes of operation for Charlie. (a) Two Wheels on Ground in Dynamically Balancing mode. (b) Four Wheels on Ground in Statically Stable Mode. (c) Four Wheels on Ground in Statically Stable/ Climbing Mode.

treads. Spacecat [21] and Epi.q-TG [22] describe robot architectures that use similar cluster wheels as in our proposed design, however neither is designed to balance dynamically on two wheels as their respective applications, lunar/mars exploration and outdoor terrain do not call for this capability which is valued in human environments.

In the following sections we first introduce a lumped parameter dynamic model for the evaluation of cluster wheel vehicles. We then make geometric and control arguments based on model analysis to select the appropriate cluster geometry. Further we describe our simulation to estimate the stability of two and three wheel clusters and present the results from simulating cluster motion. Subsequently we describe the mechanical construction and the control system architecture of the robot detailing the sensor and actuator locations. We also demonstrate basic stable obstacle traversal and examples of simulation in a video (http://youtu. be/hhfmD_FFyY4) that accompanies this paper. Note that the controller design for obstacle climbing and traversal is not the objective of this paper and we do not attempt to describe the exact method of obstacle climbing as illustrated in the video as this is part of ongoing research. Finally we conclude by explaining challenges and future research directions.

II. GEOMETRIC AND CONTROLLABILITY ANALYSIS

In this section we explore various factors informing the selection of cluster geometry. First we explain the three anticipated modes of operation of the robot, we then explain the lumped parameter model we use for our analysis. Finally we explain analytical and simulation based reasoning behind our decision to use three wheel clusters. Note that in this section and subsequent sections we define a "cluster" as consisting of the mechanical arrangement of the wheels with associated mounting structures. We define "pendulum" as the parts of the robot that do not belong to the cluster. To better illustrate our design choices in context, we present the final build of Charlie in Fig. 1.

Fig. 2 shows a simplified diagram of the robot in the three anticipated modes of operation dynamically balancing with two wheels on the ground, statically stable with four wheels on the ground (two on either side) and a climbing mode that is also statically stable with four wheels on the ground to mount curbs and stairs. While controlling the robot in each
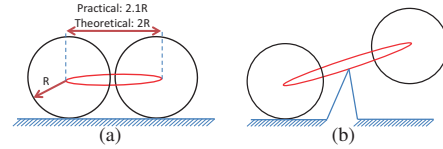

Fig. 3. Figures illustrating the optimal and non-optimal packaging of wheels. (a) Optimal inter-wheel distance. (c) Non-Optimal inter-wheel distance
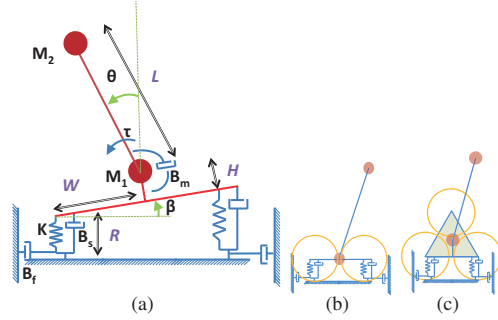

Fig. 4. Figure illustrating the dynamic model and parameters that transform it into two and three wheel clusters. (a) Lumped parameter model for cluster wheel (b) Two wheel cluster derived from the general model by setting $H = 0$, $R = W$ (c) Three wheel cluster derived from the general model by setting $H = R \times tan(\pi/6)$, $R = W$

of these modes alone is simple, it is the transitions between modes that present a design and controls challenge. As we shall see in the analytical results, the transition between these modes is not trivial and the geometry of the cluster plays a significant role in determining the feasibility of transitions. In Fig. 3(a) we show the dimensions for optimal spacing of wheels. As Fig. 3(b) shows, a deviation from this rule can result in the vehicle getting stuck on an obstacle. Keeping this in mind, we design our cluster with an inter-wheel distance of $2.1R$ where 'R' is the radius of the wheel.

A. Modelling and Controllability

To analyze the geometry of clusters that would be most suitable for our design, we employ the lumped parameter model shown in Fig. 4(a). Note the figure represents a model of the robot when on the ground in the "four wheel" mode. By appropriately setting initial conditions, this model simulates the dynamics of the robot at the moment of ground impact when transitioning between two and four wheels. Note that we omit the wheels from this model, substituting the dynamics of wheels by a dissipative damper. The intent behind this approximation is to determine if the system can be controlled by using the cluster joint alone. If indeed possible, this will allow us to control the robot in place without wheel movement on the ground which is potentially hazardous while balancing on stairs. The model also allows us simulate various cluster geometries by changing the location of the center of mass M1. For example a two wheel cluster is generated when $H = 0$, a three wheel cluster when $H = R \times tan(\pi/6)$. This transformation is illustrated in Fig. 4(b) and Fig. 4(c).

Evaluating the dynamic equations of the model described in Fig. 4(a) we obtain an 8 state (table I) non-linear system

TABLE I

STATE VARIABLES FOR MODEL IN FIG. 4(A)

Variable	Description
β	Angle between cluster and ground
θ	Angle between pendulum and vertical
xM1	Horizontal location of M1
yM1	Vertical location of M1
$\dot{\beta}$	Angular velocity between cluster and ground
$\dot{\theta}$	Angular velocity between pendulum and vertical
$\dot{xM1}$	Horizontal velocity of M1
$\dot{yM1}$	Vertical velocity of M1

(equations listed in Appendix). To evaluate the influence of cluster torque over the system dynamics we compute the controllability matrix of the linearized system in various configurations. We pay particular attention to the instant at which the cluster touches the ground as this determines if the robot is controllable at ground impact. To do this we linearize the system about the points listed in Eq. (1) and compute the controllability matrix. Here $xM1_i, yM1_i, \dot{xM1}_i, \dot{yM1}_i, \dot{\beta}_i, \dot{\theta}_i$ refer to positions and velocities at impact. Eq. (1) describes a condition where the cluster impacts the ground with a non-zero velocity or 'hard' landing. Additionally we would like the pendulum to be close to vertical to subsequently stabilize the robot in a statically stable four wheel configuration. For this we impose the conditions $\theta \to 0, \dot{\theta} \to 0$.

$$\beta \to 0, \theta \to 0, xM1 \to xM1_i, yM1 \to yM1_i, \dot{\beta} \to \dot{\beta}_i, \dot{\theta} \to 0,$$
$$\dot{xM1} \to \dot{xM1}_i, \dot{yM1} \to \dot{yM1}_i \qquad (1)$$

The controllability matrix evaluated at Eq. (1) is of the form given by Eq. (2). The functions described by the 'f' and 'g' terms are complex functions of the impact velocities. The location of the zeros in this matrix imply low control authority of the cluster torque over the 'bounce' mode of the robot. To illustrate this better we present Eqn. (3) to (5). Eq. (3) represents a general LTI system and Eq. (4) displays the fourth derivative of the state variable. Note the similarity of terms between this expression and the expression for the controllability matrix given by Eq. (5). Considering the row for vertical bounce 'yM1' in Eq. (2) we see that the first non-zero element in the row corresponds to the column of the controllability matrix given by A^3B. Correlating this with Eq. (4), we can see that the input torque 'τ' will ONLY influence the fourth derivative of 'yM1'. While the controllability matrix may appear full rank, in practice the input has insufficient control authority at impact to prevent the cluster from 'bouncing' unstable.

$$
\begin{pmatrix} \theta \\ \beta \\ xM1 \\ yM1 \\ \dot{\theta} \\ dt \\ \dot{xM1} \\ \dot{yM1} \end{pmatrix} \to
\begin{pmatrix}
0 & f1 & f2 & f3 & f4 & f5 & f6 & f7 \\
0 & f8 & f9 & f10 & f11 & f12 & f13 & f14 \\
0 & f15 & f16 & f17 & f18 & f19 & f20 & f21 \\
0 & 0 & 0 & g1 & g2 & g3 & g4 & g5 \\
f22 & f23 & f24 & f25 & f26 & f27 & f28 & f29 \\
f30 & f31 & f32 & f33 & f34 & f35 & f36 & f37 \\
f39 & f39 & f40 & f41 & f42 & f43 & f44 & f45 \\
0 & 0 & g6 & g7 & g8 & g9 & g10 & g11
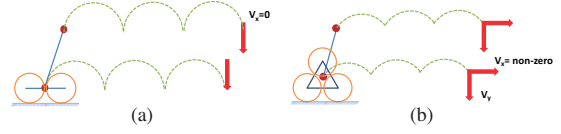\end{pmatrix} \qquad (2)
$$

Fig. 5. Cycloid traced by the mass positions (a) Two wheel cluster (b) Three wheel cluster
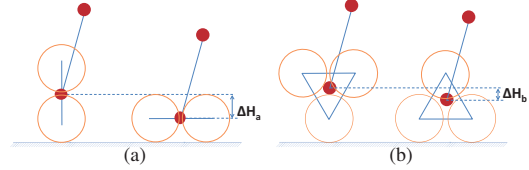

Fig. 6. Potential energy change on ground impact (a) Two wheel cluster $\Delta PE = (M1 + M2)g\Delta H_a = (M1 + M2)gR$ (b) Three wheel cluster $\Delta PE = (M1 + M2)g\Delta H_b = 0.577(M1 + M2)gR$

$$\dot{X} = AX + B\tau \qquad (3)$$
$$\ddddot{X} = A^4X + A^3B\tau + A^2B\dot{\tau} + AB\ddot{\tau} + B\dddot{\tau} \qquad (4)$$
$$C = [B|AB|A^2B...|A^{n-1}B] \qquad (5)$$

B. Selection of cluster geometry

As we have seen that the torque applied at the cluster joint is unable to control the cluster bounce at impact, the only method to ensure stable ground impact is to dissipate all kinetic energy *passively*. While employing soft viscous tires or damped suspensions are certainly an option to achieve this, the cluster geometry also has a significant impact on the passive dynamics of the cluster. Fig. 5 shows the cycloid of the mass positions with an actuated two and three wheel cluster. Note that for the two wheel cluster, **ALL** of the kinetic energy at impact is directed into the vertical uncontrollable (bounce) mode of the robot, whereas in the three wheel cluster the kinetic energy is also directed in the horizontal mode where appropriate wheel actuation may be able to dissipate it. Additionally a simple measure of the potential energy as shown in Fig. 6 between the two and three wheel configurations suggests that the three wheel cluster will have to dissipate less energy on impact when compared to the two wheel cluster. These reasons suggest that on ground impact it is easier to stabilize the three wheel cluster compared to a two wheel cluster even at the cost of small horizontal movements.

1) Simulation of cluster geometry: While the increased stability of the three wheel cluster can be explained by the analytical reasoning given above, in this section we present simulation results that support our analytical conclusions. For this we perform simulations of the cluster wheel system under the following conditions:

We initialize both two and three wheel clusters in the configuration shown in Figs. 7(a) and 7(b). Because of the dimensionality of the system involving eight state variables it becomes challenging to find initial conditions that do not lend advantages to one cluster geometry over the other. To control for this we simulate conditions that occur when

Fig. 7. Initial Conditions for two and three wheel simulations (a) Two wheel cluster (b) Three wheel cluster
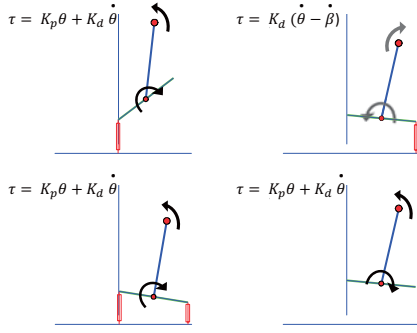

Fig. 8. Cluster controllers for various tire contact conditions: Left wheel contact, right wheel contact, two wheel contact and no contact

the clusterwheel vehicle transitions from balancing straight up to the statically stable pose. Additionally, to bias the cluster toward falling to the right we offset the pendulum mass (M_2) $10°$ to the right. We also offset the left tire spring into a compressed position that exactly balances the weight to avoid any transients. Controllers for tire contact conditions are shown in Fig. 8 illustrating the effect of applied torques. We switch between two separate expressions to generate the cluster torque (τ) required to transition from the initial conditions to a statically stable four wheel pose. Both the expressions for controller torques along with all combinations of tire ground contact are shown in Fig. 8. Note that this controller is by no means the only one that we could implement. However it is our experience that this controller adequately tests the ground impact of the clusterwheel system. Specifically this controller stresses the dissipative performance of the tire spring-dampers that is crucial to maintaining stability We vary tire stiffness (K) and damping (B_s) and monitor (a) If the clusterwheel system falls over with the pendulum hitting the ground (b) If the system does not fall over then we count the number of "bounces" on the front and back tires before the system settles into a statically stable pose. To do this we count the number of transitions between no contact to contact conditions on the left and right tires.

Note that the controller used in our simulations is by no means the only one that we could implement. However it has been our experience that this controller adequately tests the fall down of the clusterwheel system. Specifically this controller stresses the dissipative performance of the tire spring-dampers that is crucial to maintaining stability.

Fig. 9 show the results of our simulation. The numbers in the parenthesis indicate the number of No Contact to Contact transitions for the left and right tires respectively.

In addition to this the letter F denotes a failed simulation where the clusterwheel system has toppled over. Comparing the results of the simulations, we see that the two wheel cluster is more likely to be unstable. There are a number of tire stiffness and damping values for which the system has toppled over as the tire gets stiffer with low damping values. In addition, comparing the number of bounces seen on the three wheel cluster with the two wheel cluster, we see that the number of bounces of the left tire is consistently lower for the three wheel cluster. We can infer from these results that our analytical hypothesis is well supported, the two wheel cluster is at significantly greater risk of instability when compared with the three wheel cluster.

2) Size of multiwheel clusters: Previously we have seen that three wheel clusters are more stable compared to two wheel clusters both by analytic reasoning as well as by simulation. To extend this line of reasoning, the bounce behavior of four and five wheel clusters at ground impact can be more easily stabilized when compared to the three wheel cluster. However as a matter of practical construction of the clusterwheel system, we note that as more wheels are added to a cluster, the size of the cluster (e.g. width and area of the cluster) dramatically increases if we wish to keep the maximum obstacle size that can be traversed constant. The maximum obstacle size that can be traversed is related to the radius of the wheel by $x = \sqrt{3}R$. The increase in cluster size with increase in the number of wheels is shown in Figs. 10(c) to 10(e). To quantify this numerically, we define the length R_c shown in Fig. 10(b) as representative of cluster size. For various other cluster geometries $R_c = \frac{R}{\cos\left(\frac{\pi}{2} - \frac{\pi}{n}\right)}$, where '$n$' is the number of wheels. If we plot the cluster size relative to the maximum obstacle size we see that the size of the cluster increases with the number of wheels as shown in Fig. 10(f). We can see from the above analysis that the number of wheels in a cluster is a tradeoff between cluster size/complexity and stability. Therefore, as a compromise between stability at impact and cluster size we use the triangular cluster geometry for our robot Charlie

III. EXPERIMENTAL SYSTEM

In the following section we describe the electromechanical design and construction of Charlie. We first describe the design of the two drive chains in the robot, we then describe the control system architecture followed by the sensor locations and finally explain the target pitch estimation from cluster angle and the dynamically balancing controller.

A. Electromechanical Design

Fig. 11(a) shows the wheel drivetrain which consists entirely of timing belts drives. Belt drives have certain advantages over gears, belts are less prone to backlash when compared to gears and are more tolerant of misalignment. However disadvantages of belts include large packaging volume and additional tensioning devices. The reason for our decision to use belts over gears was primarily driven by a desire to avoid backlash. In a balancing machine the effects of backlash can range from benign chattering to
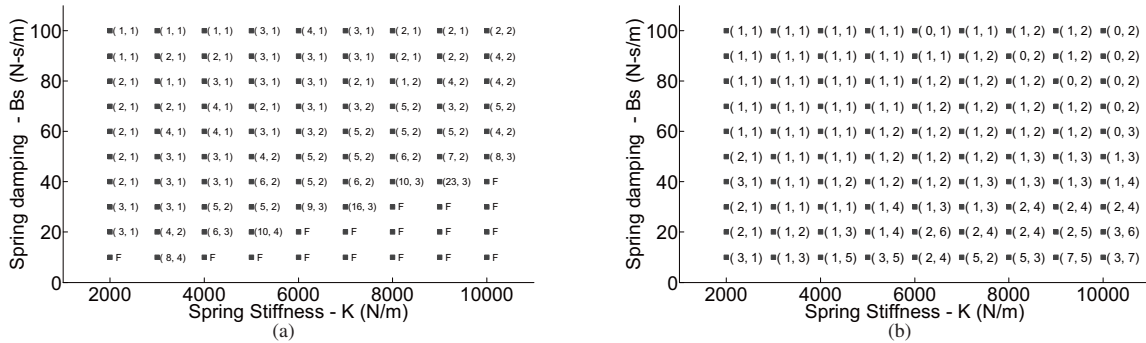
Fig. 9. Results of two and three wheel "falldown" simulations (a) Figure showing the number of left tire and right tire bounces for a TWO wheel cluster (b) Figure showing the number of left tire and right tire bounces for a THREE wheel cluster. Key: Data in parenthesis to be interpreted as (Left Wheel Transitions, Right Wheel transitions)
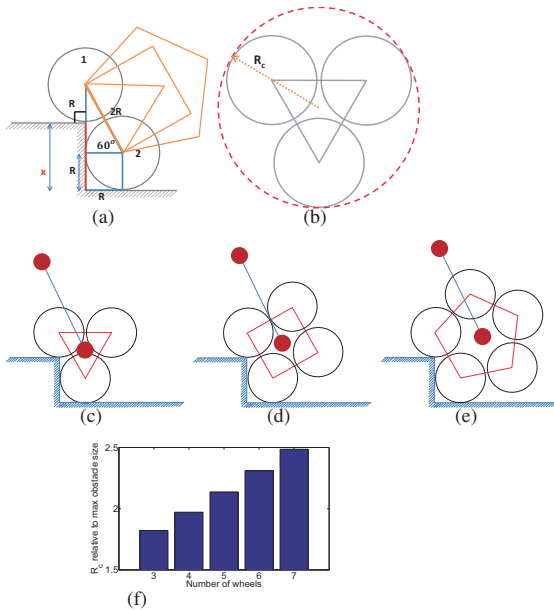

Fig. 10. (a) Figure illustrating the maximum obstacle size that can be negotiated by a cluster, here the obstacle size $x = \sqrt{3}R$ (b) Figure showing the metric used to evaluate cluster size, $R_c = \frac{R}{\cos\left(\frac{\pi}{2} - \frac{\pi}{n}\right)}$, where 'n' is the number of wheels (c)-(e) Various cluster geometries relative to obstacle size (f) Cluster size relative to maximum obstacle size $\frac{R_c}{\sqrt{3}R}$
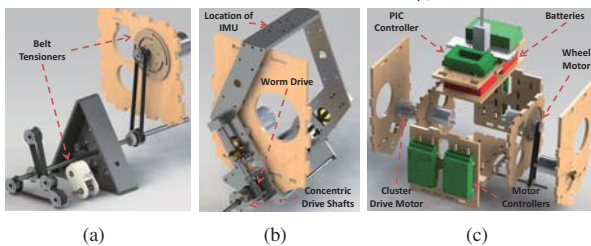

Fig. 11. Figures showing the construction of Charlie. (a) Exploded view of the drivetrain for wheels, note the tensioner on the motor and in the cluster. (b) Drivetrain for the Cluster. Note the concentric driveshafts, there exists mild frictional coupling between the cluster and wheel drivetrains. (c) Laser cut plywood housing - The motor control boards are attached to the sides, the PIC board on top with the IMU underneath the aluminum plate. The batteries, shown in red are housed above the motors.

instability. Anecdotal evidence during testing suggests that large backlash created by loose set-screws on D-shafts result in instabilities that are difficult to compensate for and lead to a failure of the balancing system. There are two tensioners in this drive system for the two belts. The belt on the motor is tensioned by mounting the motor off-center on a disc and rotating the disc until the belt is taught. The belt in the cluster is tensioned via an idler pulley on an arm that swings into the belt. The arm is adjusted with a threaded screw outside the cluster. Also note that Charlie has a single driveshaft connecting the wheels as we are interested in studying the planar dynamics of the robot.

The cluster drivetrain is designed differently from the the wheel drivetrain. The torque at the cluster has to be sufficiently large to be able to move the upper body of the robot, this requirement places restrictions on the type of gearing that can be employed. We choose a worm gear to achieve large torques at this joint, however because of this choice we trade off speed. The use of worm gears also introduces some backlash into the cluster joint, however in our experience this backlash has not seriously affected our ability to balance. Table II in the Appendix indicates the numerical value of backlash. Fig. 11(b) shows the cluster drivetrain. Also note, the cluster drivetrain is part of a larger structure enveloping the robot that lends structural rigidity, minimizing compliance. Until now we have described the two drivetrains as separate from each other. Note, however, that the drive trains pass through each other in concentric shafts and it is not surprising to find mild frictional coupling between the wheel and cluster motion. This coupling however, can be ignored as position/balance control loops wrapped around actuator motions minimize their effect.

The control architecture of Charlie is shown in Fig. 13(a). Charlie is controlled via a tether, which is suspended from the ceiling to minimize external disturbance forces. A Versalogic SBC running QNX forms the control unit, the QNX system communicates with Charlie over an RS232 link. Charlie carries on-board, J.R.Kerr motor control modules and a PIC board that reads from an accelerometer (L3G4200D) and rate-gyro (LSM303DLM) over an I^2C link. The QNX system
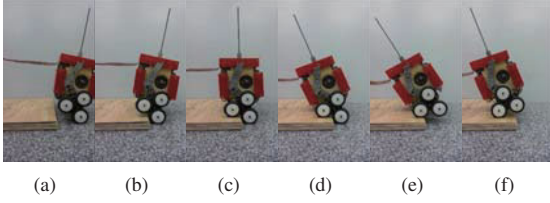
Fig. 12. Snapshots illustrating simple obstacle climbing (a)-(b),(e)-(f) Dynamically balancing two wheel mode,(c)-(d) Four Wheels on Ground in Statically Stable/ Climbing Mode
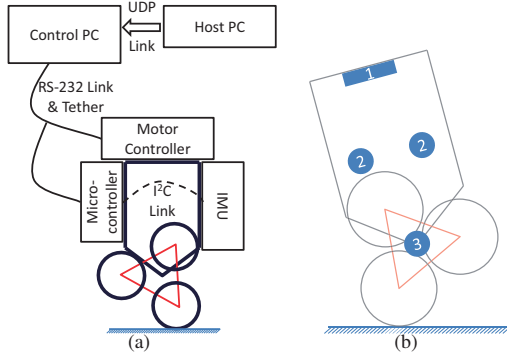

Fig. 13. (a) System Architecture, (b) Sensor Positions on Charlie. (1) Accelerometer and Rate-Gyro (2) Hall effect cluster encoders, mounted on motor (3) Wheel position optical encoder

transmits data over an UDP link to a PC running Matlab, the PC can also issue supervisory commands to the QNX system. All electronic components and motors are fixed into a plywood housing made of laser-cut plywood.

Fig. 13(b) shows the location of various sensors on Charlie. The rate-gyro and the accelerometer are mounted on the aluminum structure that is part of the cluster drivetrain to minimize compliance. The wheel optical encoder is mounted on the shaft driving the wheels. It has been our experience that mounting this encoder at the motor results in reduced stability margins (lower max gains) possibly due to the compliance in the timing belt between the motor and shaft. The cluster encoder is however mounted on the motors directly as a time delay in the control of the cluster joint is less critical given its slower actuation speed.

B. Pitch Angle Estimation & Balancing controller

Fig. 14 shows the pitch angles corresponding to the various cluster angles. While obtaining the desired pitch from the kinematic relationships is relatively simple, we use values determined by measuring the pitch angle at zero moment points for various cluster angles. The pitch angles obtained in this way control for deviation from theoretical values due to any offset masses in the structure of the robot.

While balancing dynamically on two wheels, the robot is stabilized using a full-state controller. The controller is of the form

$$V_{uc} = k_{p\phi}(\phi - \phi_{des}) + k_{d\phi}\dot{\phi} + k_{p\theta}(\theta - \theta_{des}) + k_{d\theta}\dot{\theta} \quad (6)$$

$$V = V_{uc} + V_{fc}sign(V_{uc}) \quad (7)$$

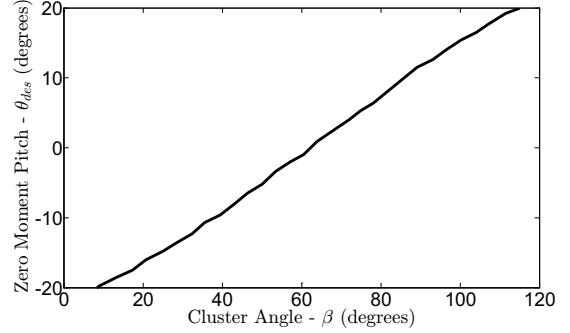Fig. 14. Plot of θ_{des} determined by measuring the pitch angle at zero moment points

where $k_{p\phi}$, $k_{d\phi}$, $k_{p\theta}$, $k_{d\theta}$ are the gains associated with wheel position, wheel angular velocity, pendulum angular position (tilt), pendulum angular velocity (rate of tilt) respectively and the value of θ_{des} is given by Eq. (7). V_{fc} is a variable friction compensation term that is determined by a limit cycle compensation algorithm [23] and 'V' is the PWM modulated voltage that is applied to the motors.

IV. CONCLUSIONS AND FUTURE WORK

In this paper we describe the effect of cluster geometry on the dynamics of a clusterwheel balancing robots. We first propose a dynamic lumped model for cluster wheel architectures. Using this model we then present analytic results based on controllability and energy dissipation arguments. Our results indicate that as the number of wheels in a cluster increase, it becomes easier to stabilize the system on impact with the ground. Next we simulate two and three wheel cluster geometries with a variety of tire parameters to test and verify our energy dissipation hypothesis. We then discuss practical implications of increasing the number of wheels in a cluster, pointing out that this will lead to an increase in cluster size and mechanical complexity. We then conclude that a three wheel cluster is ideally suited for our application. Subsequently we describe the electromechanical design and construction of our cluster wheel robot "Charlie", including design measures to minimize compliance and backlash.

A. Video of balancing robot

Finally we also submit a video demonstration (http://youtu.be/hhfmD_FFyY4) of teleoperated object traversal using the robot. Additionally, for reasons of clarity we also include clips from our simulation of clusterwheel architectures.

This paper outlines the beginnings of our investigation into clusterwheel robots. Ongoing investigations explore the development of controllers for switching between two and three wheel modes as well as obstacle traversal. Our long term objective is to develop a stable control system to allow dynamic balancing while negotiating planar obstacles like curbs and stairs.

APPENDIX

Equations representing the dynamics of a general cluster-wheel Eqn. (8) to (11) robot as shown in Fig. 4(a).Table III lists the various parameters of the model in addition to the state variables described in table I.

$$-\frac{Bm\dot{\beta}}{IM2+L^2M2}+\frac{Bm\dot{\theta}}{IM2+L^2M2}-\frac{gLM2\sin(\theta)}{IM2+L^2M2}+\ddot{\theta}+\frac{\tau}{IM2+L^2M2}=0 \tag{8}$$

$$\ddot{\beta}+\frac{2BfHyM1\dot{\beta}\cos(\beta)}{IM1}+\frac{2BfyM1x\dot{M1}}{IM1}+\frac{Bm\dot{\beta}}{IM1}-\frac{Bm\dot{\theta}}{IM1}+\frac{2BsH^2\dot{\beta}\sin^2(\beta)}{IM1}+\frac{2BsH\sin(\beta)y\dot{M1}}{IM1}$$

$$+\frac{2BsW^2\dot{\beta}\cos^2(\beta)}{IM1}-\frac{H^2K\sin(2\beta)}{IM1}-\frac{2HKy0\sin(\beta)}{IM1}+\frac{2HKyM1\sin(\beta)}{IM1}+\frac{KW^2\sin(2\beta)}{IM1}-\frac{\tau}{IM1}=0 \tag{9}$$

$$\frac{2BfH\dot{\beta}\cos(\beta)}{M1+M2}+\frac{2Bfx\dot{M1}}{M1+M2}-\frac{BmLM2\dot{\beta}\cos(\theta)}{(M1+M2)\left(IM2+L^2M2\right)}+\frac{BmLM2\dot{\theta}\cos(\theta)}{(M1+M2)\left(IM2+L^2M2\right)}$$

$$-\frac{gL^2M2^2\sin(\theta)\cos(\theta)}{(M1+M2)\left(IM2+L^2M2\right)}+\frac{LM2\tau\cos(\theta)}{(M1+M2)\left(IM2+L^2M2\right)}+\frac{LM2\dot{\theta}^2\sin(\theta)}{M1+M2}+x\ddot{M1}=0 \tag{10}$$

$$-\frac{BmLM2\dot{\beta}\sin(\theta)}{(M1+M2)\left(IM2+L^2M2\right)}+\frac{BmLM2\dot{\theta}\sin(\theta)}{(M1+M2)\left(IM2+L^2M2\right)}+\frac{2BsH\dot{\beta}\sin(\beta)}{M1+M2}+\frac{2Bsy\dot{M1}}{M1+M2}$$

$$-\frac{gL^2M2^2\sin^2(\theta)}{(M1+M2)\left(IM2+L^2M2\right)}+\frac{gM1}{M1+M2}+\frac{gM2}{M1+M2}-\frac{2HK\cos(\beta)}{M1+M2}$$

$$+\frac{LM2\tau\sin(\theta)}{(M1+M2)\left(IM2+L^2M2\right)}-\frac{2Ky0}{M1+M2}+\frac{2KyM1}{M1+M2}-\frac{LM2\dot{\theta}^2\cos(\theta)}{M1+M2}+y\ddot{M1}=0 \tag{11}$$

TABLE II
NUMERICAL VALUES FOR PARAMETERS

Parameter	Value
Wheel Drivetrain Gearing Ratio	73.10
Cluster Drivetrain Gearing Ratio	494
Backlash in Cluster Joint	$2.21°$
Motor Max Torque (Cluster and Wheel)	52.03mNm
Wheel Max Speed (no load)	264.56 rpm
Cluster Max Speed (no load)	27.85 rpm
Motor Driving Voltage	20V
L3G4200D Accelerometer	Fullrange:$250°s^{-1}$; Sensitivity:$8.75°\times10^{-3}s^{-1}$
LSM303DLM rate-gyro	Fullrange:$\pm2g$, Resolution: 12 bits
Wheel Optical Encoder	2000cpr
Cluster Hall effect Encoder	64cpr
Center of Gravity	19.5×10^{-2}m above axle
Natural frequency	$1.128Hz$
Sampling Frequency	$100Hz$

TABLE III
VARIABLES IN LUMPED PARAMETER MODEL

Variable	Decription
M1, IM1	Mass and Inertia of Pendulum
M2, IM2	Mass and Inertia of Cluster
Bs,Bf,Bm	Damping at tires, horizontal damper and the cluster-pendulum joint
K	Spring constant of tires
L	Length of pendulum
H	Location of center of mass of cluster from the midpoint of the line connecting two wheels
R	Radius of tire

REFERENCES

[1] F. Grasser, A. D"Arrigo, S. Colombi, and A. Rufer, "Joe: a mobile, inverted pendulum," *Industrial Electronics, IEEE Transactions on*, vol. 49, no. 1, pp. 107–114, Feb.

[2] H. G. Nguyen, A. J. Morrell, B. K. Mullens, A. A. Burmeister, S. Miles, C. N. Farrington, A. K. Thomas, and D. W. G. E, "Segway robotic mobility platform," in *SPIE Mobile Robots XVII*, 2004.

[3] http://www.segway.com/, uRL http://www.segway.com/.

[4] T. B. Lauwers, G. A. Kantor, and R. L. Hollis, "A dynamically stable single-wheeled mobile robot with inverse mouse-ball drive," in *Proc. of 2006 IEEE International Conference on Robotics and Automation, May 15-19, 2006, Pages:2884*, 2006, p. 2889.

[5] R. Nakajima, T. Tsubouchi, S. Yuta, and E. Koyanagi, "A development of a new mechanism of an autonomous unicycle," in *Intelligent Robots and Systems, 1997. IROS '97., Proceedings of the 1997 IEEE/RSJ International Conference on*, vol. 2, 1997, pp. 906–912 vol.2.

[6] Y. Ha and S. Yuta, "Trajectory tracking control for navigation of self-contained mobile inverse pendulum," in *Intelligent Robots and Systems '94. 'Advanced Robotic Systems and the Real World', IROS '94. Proceedings of the IEEE/RSJ/GI International Conference on*, vol. 3, 1994, pp. 1875–1882 vol.3.

[7] [Online]. Available: http://www.dekaresearch.com/ibot.shtml

[8] [Online]. Available: http://www.ibotnow.com/

[9] B. N. Dean L. Kamen, M. N. Robert R. Ambrogi, M. N. John D. Heinzmann, F. N. Richard Kurt Heinzmann, C. N. David Herr, and M. N. John B. Morrell, "Control of a balancing personal vehicle," US Patent US 6 799 649, 10 05, 2004.

[10] M. N. John B. Morrell, W. M. John M. Kerwin, B. N. Dean L. Kamen, M. N. Robert R. Ambrogi, S. N. Robert J. Duggan, F. N. Richard K. Heinzmann, and P. N. Brian R. Key, "System and method for stair climbing in a cluster-wheel vehicle," US Patent US 6 311 794, 11 06, 2001.

[11] M. N. John B. Morrell and M. N. John M. Kerwin, "Methods for stair climbing in a cluster-wheel vehicle," US Patent US 6 443 251, 09 03, 2002.

[12] M. N. John B Morrell and M. N. John M. Kerwin, "Operating modes for stair climbing in a cluster-wheel vehicle," US Patent US 6 343 664, 02 05, 2002.

[13] M. N. John B. Morrell and M. N. John M Kerwin, "Mechanism for stair climbing in a cluster-wheel vehicle," US Patent US 6 615 938, 09 09, 2003.

[14] P. Bartlett, D. Wettergreen, and W. R. L. Whittaker, "Design of the scarab rover for mobility and drilling in the lunar cold traps," in *International Symposium on Artificial Intelligence, Robotics and Automation in Space*, February 2008.

[15] R. Quinn, J. Offi, D. Kingsley, and R. E. Ritzmann, "Improved mobility through abstracted biological principles," in *Intelligent Robots and Systems, 2002. IEEE/RSJ International Conference on*, vol. 3, pp. 2652–2657 vol.3.

[16] M. Lauria, Y. Piguet, and R. Siegwart, "Octopus - an autonomous wheeled climbing robot," in *In Proceedings of the Fifth International Conference on Climbing and Walking Robots, Published by Professional Engineering Publishing Limited, Bury St Edmunds and*, 2002.

[17] M. Guarnieri, P. Debenest, T. Inoh, K. Takita, H. Masuda, R. Kurazume, E. Fukushima, and S. Hirose, "Helios carrier: Tail-like mechanism and control algorithm for stable motion in unknown environments," in *Robotics and Automation, 2009. ICRA '09. IEEE International Conference on*, may 2009, pp. 1851 –1856.

[18] D. Helmick, S. Roumeliotis, M. McHenry, and L. Matthies, "Multi-sensor, high speed autonomous stair climbing," in *Intelligent Robots and Systems, 2002. IEEE/RSJ International Conference on*, vol. 1, pp. 733–742 vol.1.

[19] C. Marques, J. Cristovao, P. Lima, J. Frazao, I. Ribeiro, and R. Ventura, "Raposa: Semi-autonomous robot for rescue operations," in *Intelligent Robots and Systems, 2006 IEEE/RSJ International Conference on*, Oct., pp. 3988–3993.

[20] W. Lee, S. Kang, M. Kim, and K. Shin, "Rough terrain negotiable mobile platform with passively adaptive double-tracks and its application to rescue missions," in *Robotics and Automation, 2005. ICRA 2005. Proceedings of the 2005 IEEE International Conference on*, April, pp. 1591–1596.

[21] M. Lauria, F. Conti, P.-A. Musli, M. van Winnendael, R. Bertrand, and R. Siegwart, "Design and Control of an Innovative Micro-Rover," in *None*, 1998. [Online]. Available: http://www.estec.esa.nl/conferences/astra98

[22] L. Bruzzone, R. Oderio, G. Quaglia, and R. Razzoli, "Experimental assessment and evolution perspectives of the epi.q mobile robot architecture," in *XX Congresso dell'Associazione Italiana di Meccanica Teorica e Applicata AIMETA 2011*, 2011. [Online]. Available: http://porto.polito.it/2487001/

[23] H. Vasudevan, A. M.Dollar, and J. B.Morrell, "Energy-based limit cycle compensation for dynamically balancing wheeled inverted pendulum machines," in *Dynamic Systems and Control Conference, 2013. DSCC '2013. Proceedings. ASME 2013*, 2013.